Origin of the different reactivity of the high-valent coinage-metal complexes $[RCu^{III}Me_3]^-$ and $[RAg^{III}Me_3]^-$ (R = allyl)

Thomas Auth,[a]* Christopher J. Stein,[b]* Richard A. J. O'Hair,[c] and Konrad Koszinowski[a]

[a] Institut für Organische und Biomolekulare Chemie, Universität Göttingen, Tammannstr. 2, 37077 Göttingen, Germany

[b] Theoretical Physics and Center for Nanointegration Duisburg-Essen (CENIDE), University of Duisburg-Essen, 47048 Duisburg, Germany

[c] School of Chemistry and Bio21 Molecular Science and Biotechnology Institute, University of Melbourne, 30 Flemington Rd, Parkville, Victoria 3010, Australia

E-mail: thomas.auth@chemie.uni-goettingen.de, christopher.stein@uni-due.de

Abstract: High-valent tetraalkylcuprates(III) and -argentates(III) are key intermediates of copper- and silver-mediated C−C coupling reactions. Here, we investigate the previously reported contrasting reactivity of $[RM^{III}Me_3]^-$ complexes (M = Cu, Ag and R = allyl) with energy-dependent collision-induced dissociation experiments, advanced quantum-chemical calculations and kinetic computations. The gas-phase fragmentation experiments confirmed the preferred formation of the $[RCuMe]^-$ anion upon collisional activation of the cuprate(III) species, consistent with a homo-coupling reaction, whereas the silver analogue primarily yielded $[AgMe_2]^-$, consistent with a cross-coupling reaction. For both complexes, density functional theory calculations identified one mechanism for homo coupling and four different ones for cross coupling. Of these pathways, an unprecedented concerted *outer-sphere* cross coupling is of particular interest, because it can explain the formation of $[AgMe_2]^-$ from the argentate(III) species. Remarkably, the different C−C coupling propensities of the two $[RM^{III}Me_3]^-$ complexes become only apparent when properly accounting for the multi-configurational character of the wave function for the key transition state of $[RAgMe_3]^-$. Backed by the obtained detailed mechanistic insight for the gas-phase reactions, we propose that the previously observed cross-coupling reaction of the silver complex in solution proceeds via the *outer-sphere* mechanism.

Introduction

Copper-mediated C−C coupling reactions play an outstanding role in the field of organic synthesis.[1,2] In contrast, analogous silver-mediated transformations are by far not that well established,[3,4] but the potential of silver to mediate the formation of carbon−carbon bonds has become a greater focus of attention just recently.[5–10] While the usefulness of organoargentates in stoichiometric alkylation reactions was questioned on the basis of theoretical calculations and gas-phase experiments in the past,[11,12] a collaboration between a few of us and the Ogle group has recently shown that a $LiAgMe_2{\cdot}LiI$ reagent indeed undergoes a cross-coupling reaction with allyl iodide in THF.[7] By means of rapid-injection (RI) NMR spectroscopy, the argentate(III) complex $[RAgMe_3]^-$ (R = allyl) formed from $[AgMe_2]^-$ was identified as the key intermediate in this reaction. This provides experimental evidence that the silver-mediated transformation proceeds *via* a I/III oxidation state sequence just as its copper analogue.[13] In line with this, Ribas, Roithová and co-workers have demonstrated that silver(I)-catalyzed cross-coupling reactions involve 2-electron redox processes[5,6] similar to the corresponding copper(I) chemistry.[1,14,15]

Despite these similarities between copper- and silver-mediated C−C coupling reactions, the reaction between $LiMMe_2{\cdot}LiI$ and RX reveals a striking difference for M = Cu and Ag (X = Cl, I for M = Cu, Ag, respectively). As Bartholomew *et al.* have reported in an RI-NMR spectroscopic study, the reactive intermediate for the formation of 1-butene starting from $LiCuMe_2{\cdot}LiI$ and allyl chloride is the neutral $[RCuMe_2]$ π-allyl compound,[13] whereas reductive elimination of 1-butene from the ate complex $[RAgMe_3]^-$ was found for the corresponding $LiAgMe_2{\cdot}LiI$/RI reaction system (Figure 1).[7] In the reaction solution of the organocuprate, the analogue ate complex $[RCuMe_3]^-$ was detected as well, but the results of the RI-NMR spectroscopic experiments indicated that the latter reacted towards the neutral $[RCuMe_2]$ species and did not undergo a C−C coupling reaction (Figure 1, top).[13]

The observations for the copper-mediated allylic alkylation in solution are fully in accordance with theoretical and gas-phase investigations on the reactivity of $[RCuMe_2]$, which ascertained that the latter efficiently mediates cross coupling.[11,12] In addition, gas-phase fragmentation experiments on $[RCuMe_3]^-$ mainly resulted in the formation of $[RCuMe]^-$ (Figure 1, top).[16] This fragmentation channel is consistent with homo coupling, *i.e.*, the formation of ethane, which was calculated to feature a lower barrier than the cross-coupling reaction for the cuprate(III) complex.[16] Consequently, the reactivity studies on isolated $[RCuMe_3]^-$ suggest as well that the observed cross coupling between $LiCuMe_2{\cdot}LiI$ and allyl chloride in solution must proceed *via* the neutral $[RCuMe_2]$ compound. Gas-phase fragmentation experiments on $[RAgMe_3]^-$ also support the findings of the RI-NMR study regarding the mechanism of the silver-mediated allylic alkylation. Collisional heating of this heteroleptic argentate(III) species predominantly yielded the product ion $[AgMe_2]^-$ (Figure 1, bottom), which is consistent with cross coupling, *i.e.*, the formation of 1-butene.[7] Thus, the gas-phase results corroborate that the $[RAgMe_3]^-$ complex indeed is the key intermediate of the cross-coupling reaction in solution.

In summary, both copper and silver mediate the methylation of an unsubstituted allyl ligand in THF *via* a complex featuring the metal center in the oxidation state III.[7,13] However, dependent on the coinage metal, the latter is an $[RMMe_2]$ π-allyl complex for M = Cu and a $[RMMe_3]^-$ compound for M = Ag.[17] The structure and reactivity of $[RMMe_2]$ (M = Cu, Ag) have been carefully investigated by quantum-chemical calculations already and qualitatively similar results were obtained for both complexes.[11,12] In contrast, the details of the reactivity of the key interme-

diate $[RMMe_3]^-$ for M = Ag have not been clarified. In this regard, the origin of the qualitatively different reactivities of $[RMMe_3]^-$ for M = Cu and Ag upon collisional activation is of particular interest. Moreover, understanding the cross-coupling reactivity of $[RAgMe_3]^-$ is also crucial for predicting whether this type of argentate(III) complex promotes a different regio- and stereoselectivity in comparison to the C–C coupling mechanisms identified for various $[R^YCuMeZ]$ π-allyl species (R^Y = substituted allyl; Z = Me, CN).[18,19]

In this study, we first performed energy-dependent collision-induced dissociation (CID) experiments on $[RCuMe_3]^-$ and $[RAgMe_3]^-$ under comparable conditions in order to characterize the previously reported different gas-phase reactivity of these complexes[7,16] in greater detail. We then explored in detail the potential energy surfaces for the observed fragmentation channels using density functional theory (DFT) geometry optimizations and consecutive DLPNO-CCSD(T) as well as CASPT2 single point energy calculations. Finally, we conducted statistical rate theory calculations on the basis of the results obtained from the quantum-chemical calculations to compare the experimental and theoretical results in a more direct manner. By this means, we elucidate the intrinsic reactivity of the two coinage metallate(III) C–C coupling intermediates in depth and provide a mechanistic understanding of the origin of their different chemical behaviour. At the same time, our experimental data on the reactivity of well-defined ionic systems allows us to probe the accuracy and limits of the applied state-of-the art electronic-structure methods with respect to the calculation of reaction barriers of synthetically relevant and theoretically challenging high-valent transition-metal complexes.

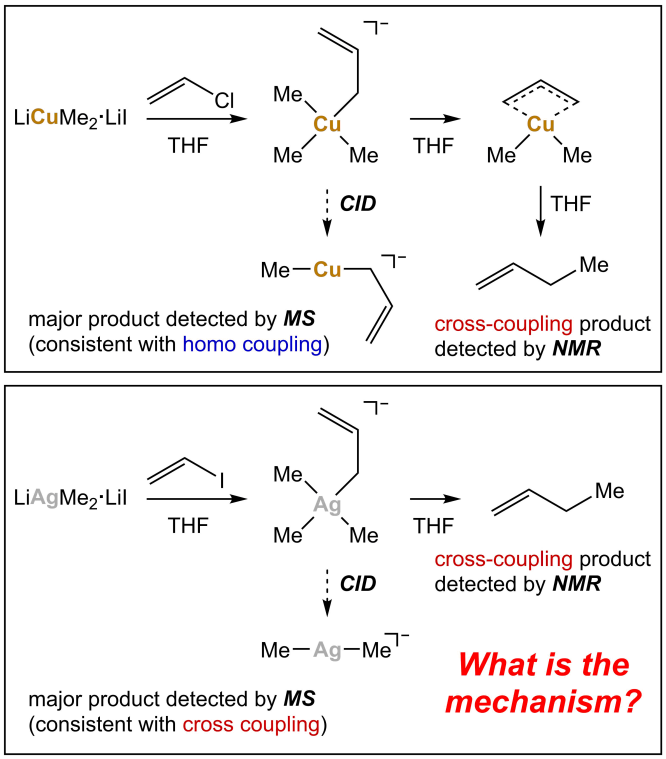

Figure 1. Mechanistic details of copper- (top) and silver-mediated (bottom) allylic methylation reactions obtained from NMR experiments, and gas-phase reactivity of the involved organometallate(III) complexes upon collision-induced dissociation (CID). The origin of the cross-coupling capability of the argentate(III) species has not been investigated so far.

Results and Discussion

Mass-Spectrometric Measurements

Following the work of Putau *et al.*[16] and Weske *et al.*,[7] the gaseous ions $[RCuMe_3]^-$ and $[RAgMe_3]^-$ (R = allyl) were obtained by electrospray ionization of reaction solutions of CuCN/3 MeLi/RCl and AgCN/2 MeLi/0.5 RI in THF, respectively (Figures S1 and S2; for experimental details, see the Supporting Information). In accordance with these previous studies, for both ions, collisional activation by means of a quadrupole time-of-flight (Q-TOF) mass spectrometer yielded the species $[RMMe]^-$ and $[MMe_2]^-$ (M = Cu, Ag; Figure S3; for experimental details, see the Supporting Information). Moreover, in the case of $[RCuMe_3]^-$, $[CuMe_3]^{\cdot -}$ was found as a minor product, which was not observed in the analogous quadrupole ion trap (QIT) fragmentation experiments.[16] Such a difference between the results from Q-TOF and QIT CID experiments is not unexpected, because Q-TOF fragmentation experiments are associated with higher collision energies and shorter reaction times between collisional activation and ion detection referred to as experimental time scale or kinetic window, τ (for details on τ of the conducted Q-TOF CID experiments, see the Supporting Information).[20,21]

As neutral fragments cannot be detected within mass-spectrometric CID experiments, the reaction mechanism behind the occurrence of the $[RMMe]^-$ and $[MMe_2]^-$ ions is not directly obvious. DFT calculations suggest that the formation of $[RCuMe]^-$ and $[CuMe_2]^-$ can be attributed to the reductive elimination of ethane (homo coupling) and 1-butene (cross coupling) from $[RCuMe_3]^-$, respectively (Eqs. 1a and 2a with M = Cu).[16,22–24] However, the generation of these fragment ions is also conceivable *via* twofold consecutive homolytic bond dissociations including the release of the corresponding organyl radicals and the occurrence of a transient threefold-coordinated open-shell organocuprate species (Eqs. 1b, 2b and 2c with M = Cu).[25–27] So far, the energy profiles of the two-step dissociation processes have not been characterized by quantum-chemical calculations, and thus, their relevance is unclear. Nevertheless, the detection of the single bond fission product $[CuMe_3]^{\cdot -}$ (first step of Eq. 2b with M = Cu) in the present experiments indicates that the formation of $[CuMe_2]^-$ according to Eq. 2b is also feasible. Recently, the ability to undergo reductive elimination has also been demonstrated for the homoleptic argentate complex $[AgMe_4]^-$ by quantum-chemical calculations.[7] This finding together with the absence of single bond fission products for the collisional activation of $[RAgMe_3]^-$ in the Q-TOF instrument suggests the direct formation of $[RAgMe]^-$ and $[AgMe_2]^-$ *via* C—C coupling reactions (Eqs. 1a and 2a with M = Ag). However, knowledge about the energy profiles for the alternative stepwise generation of these species (Eqs. 1b, 2b and 2c with M = Ag) is necessary to confidently exclude a consecutive bond dissociation pathway.

In line with the previous studies,[7,16] the results of our directly comparable Q-TOF fragmentation experiments on $[RCuMe_3]^-$ and $[RAgMe_3]^-$ for different collision energies unambiguously reveal the contrasting reactivity of these compounds (Figure 2). While the copper complex clearly favors the generation of $[RCuMe]^-$ over a broad range of the collision energy parameter E_{LAB}, the silver species predominantly yields $[AgMe_2]^-$ with an increasing $[AgMe_2]^-/[RAgMe]^-$ product ratio for increasing E_{LAB}. In the case of $[RCuMe_3]^-$, the $[RCuMe]^-/[CuMe_2]^-$ product ratio decreases towards 1 with increasing E_{LAB} (Figure 2, top). Such a behaviour has not been observed in the QIT CID study of Putau *et al.*,[16] in which a product ratio of about 4 was measured at complete fragmentation of the precursor ions. Most likely, again, this discrepancy can be attributed to the

different conditions for Q-TOF and QIT fragmentation experiments. The origin for the deviating observations depending on the experimental setup will be discussed in more detail on the basis of our computational results.

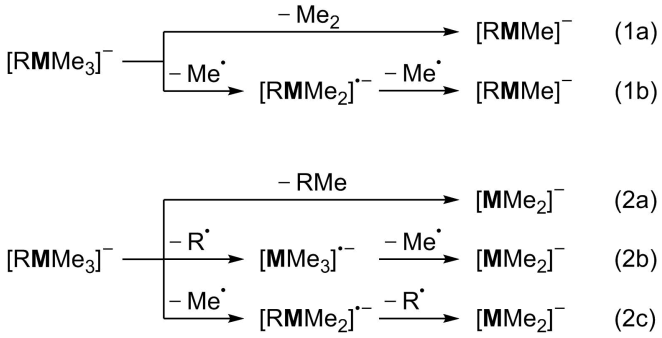

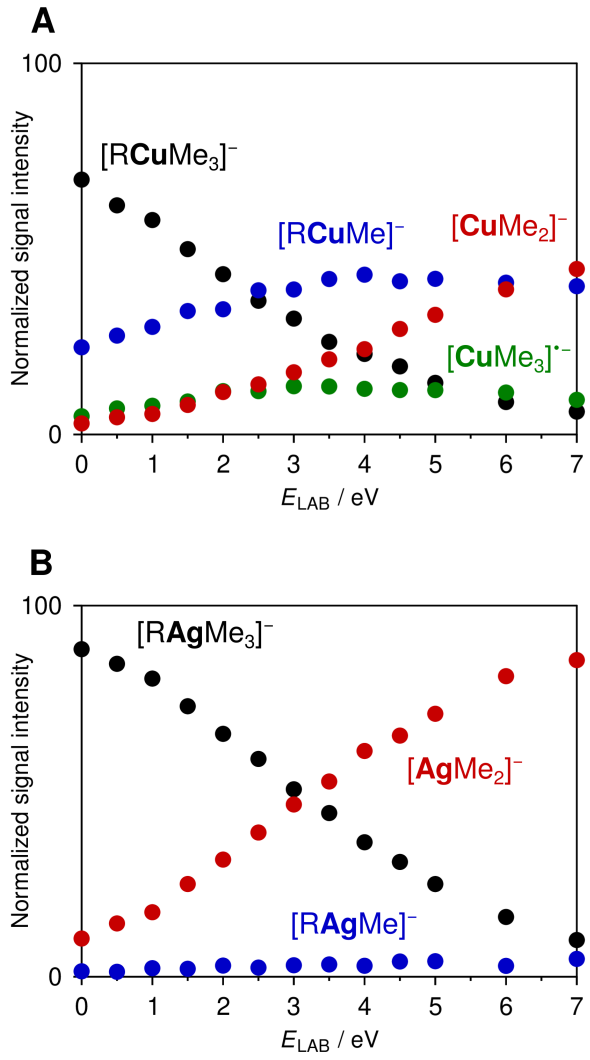

Figure 2. Normalized signal intensities of mass-selected (A) $[RCuMe_3]^-$ and (B) $[RAgMe_3]^-$ (both black) and their fragment ions (R = allyl) as a function of the collision energy parameter E_{LAB}. The fragment ions correspond to a net loss of Me_2 (blue), RMe (red) and $R^{\bullet}$ (green).

Calculated Reaction Pathways

In order to understand the different unimolecular reactivity of $[RCuMe_3]^-$ and $[RAgMe_3]^-$ (R = allyl), the C—C coupling reaction space of both species according to Eqs. 1a and 2a as well as their twofold consecutive homolytic bond dissociations (Eqs. 1b, 2b and 2c) were explored by means of PBE-D3BJ/VTZ-PP calculations (abbreviated as PBE-D3BJ in the following; for computational details, see the Supporting Information).[28–31] For both complexes, which have a similar square-planar equilibrium geometry featuring an η^1-allyl ligand pointing away from the coordination plane, five different concerted C—C coupling reaction pathways were identified (Figure 3, Figures S4 and S5): one homo-coupling pathway, which involves two neighbouring methyl groups approaching each other to afford ethane and the linear $[RMMe]^-$ complex (R = η^1-allyl) and four different cross-coupling pathways leading to the formation of 1-butene and the linear $[MMe_2]^-$ species (M = Cu, Ag). One cross-coupling pathway, which is termed *regular* in the following, corresponds to the C—C bond formation between the allyl α-C atom and a neighbouring methyl group and thus, resembles a typical reductive elimination step similar to homo coupling. Two further cross-coupling pathways are associated with 5-membered transition state (TS) structures resulting from the attack of the allyl γ-C atom at the neighbouring or opposite methyl group, which are termed *cis-cyclic* and *trans-cyclic*, respectively. The last cross-coupling pathway identified also involves the C—C bond formation between the allyl γ-C atom and a neighbouring methyl group. However, this time, the η^1-coordination of the allyl ligand is lost prior to the bond formation and we term this pathway *outer-sphere* in the following.[32–34] The presented homo- and regular cross-coupling pathways were already taken into account for $[RCuMe_3]^-$ in the context of the DFT calculations of Putau *et al.*[16] and moreover, are mechanistically similar to the reductive elimination of ethane from $[AgMe_4]^-$, which was characterized by quantum-chemical calculations by Weske *et al.*[7] In contrast, the possibility of heteroleptic square-planar coinage metal complexes like $[RMMe_3]^-$ (M = Cu, Ag; R = η^1-allyl) to undergo a *cyclic* or *outer-sphere* C—C coupling reaction has not been examined before.

In addition, energy-minimum structures for the transient species $[RMMe_2]^{\cdot-}$ and $[MMe_3]^{\cdot-}$ corresponding to the alternative two-step generation of $[RMMe]^-$ and $[MMe_2]^-$ from $[RMMe_3]^-$ (M = Cu, Ag; R = η^1-allyl; Eqs. 1b, 2b and 2c) were obtained (Figure 4). These structures are T-shaped and thus, *cis* and *trans* isomers exist for $[RMMe_2]^{\cdot-}$. Such a coordination geometry has also been found with DFT calculations for the neutral coinage-metal(III) complexes $[AgMe_3]$ and $[AuMe_3]$ previously,[7,11] whereas the analogous $[CuMe_3]$ species has been shown to spontaneously decompose into [CuMe] and ethane.[35,36] To provide a complete picture of the unimolecular reaction space of $[RCuMe_3]^-$ and $[RAgMe_3]^-$, PBE-D3BJ geometries of the neutral product complexes, $[RMMe_2]$ and $[MMe_3]$, resulting from the heterolytic bond dissociation reactions of their parent compounds, were also calculated. For $[RMMe_2]$, the well-known η^3-allyl complexes[11,12] were obtained and likewise, the aforementioned T-shaped structures could be reproduced for $[MMe_3]$ (M = Cu, Ag). As stated above, the lowest energy configuration of the $[CuMe_3]$ complex corresponds to a homo-coupling TS structure ($[CuMe_3]^‡$) and thus, the R^- loss of $[RCuMe_3]^-$ would be accompanied by the formation of [CuMe] and ethane in a concerted fashion. Most likely, the actual barrier of this reaction will not be located in the dissociation limit of the $[CuMe_3]^‡$ and R^- fragments, but rather at a certain distance where the stabilization of the T-shaped $[CuMe_3]$ unit by the allyl anion is not sufficient anymore, but the ion—induced dipole interaction is still significant. Consequently, the $[CuMe_3]^‡ + R^-$ dissociation limit is expected to represent the upper bound of the threshold energy for the concerted R^--loss/homo-coupling process starting from $[RCuMe_3]^-$.

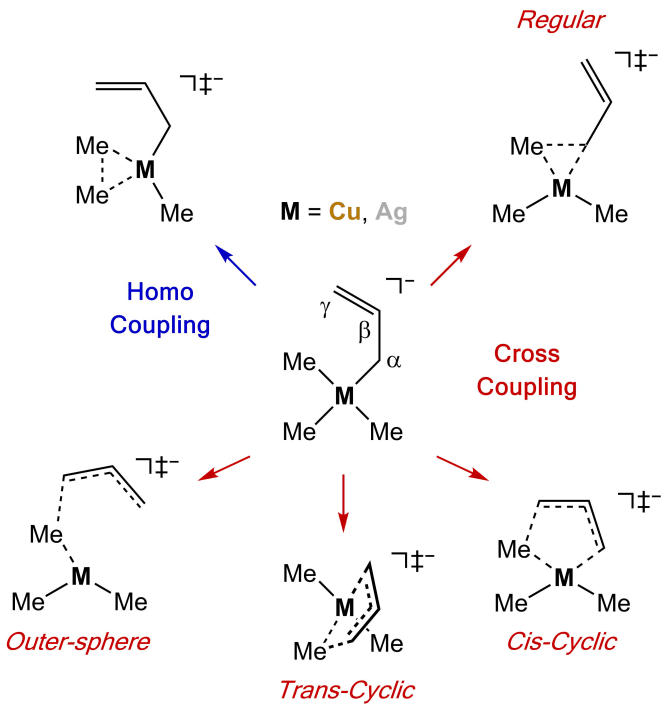

Figure 3. Schematic representation for the C—C coupling reactivity of $[RCuMe_3]^-$ and $[RAgMe_3]^-$ (R = η^1-allyl) showing the calculated transition state structures corresponding to homo- and cross-coupling reactions.

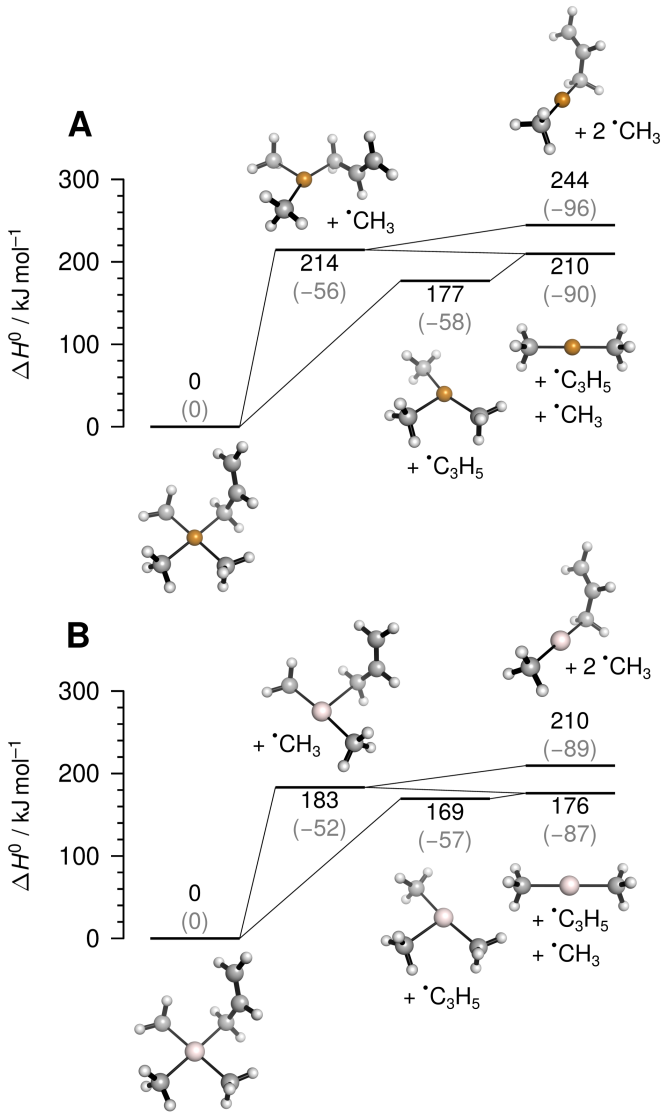

Figure 4. Energy diagrams for the twofold consecutive homolytic bond dissociations of (A) $[RCuMe_3]^-$ and (B) $[RAgMe_3]^-$ (R = η^1-allyl; according to Eqs. 1b, 2b and 2c) obtained from DLPNO-CCSD(T)//PBE-D3BJ calculations. Relative entropies (multiplied with $-T$, for T = 298.15 K) are given in brackets. Only the energetically most favorable isomer is considered for each of the $[RMMe_2]^{\bullet-}$ complexes.

DLPNO-CCSD(T) Potential Energy Surfaces

According to our DLPNO-CCSD(T)/VQZ-PP//PBE-D3BJ calculations (abbreviated as DLPNO-CCSD(T)//PBE-D3BJ in the following; for computational details, see the Supporting Information),[37–39] all of the identified C−C coupling pathways of $[RCuMe_3]^-$ and $[RAgMe_3]^-$ feature a pronounced reaction barrier, which corresponds to the C−C bond formation accompanied by the change of the oxidation state of the metal from +III to +I (Figures S4 and S5). The calculated reaction barriers, $\Delta H^{0\ddagger}$, for homo and *regular* cross coupling of $[RCuMe_3]^-$ are 125 and 150 kJ mol^{-1}, respectively (Figure 5, Table S1), which is in good agreement with the DFT results from Putau *et al.*[16] The hitherto unconsidered *cis-cyclic*, *trans-cyclic* and *outer-sphere* cross-coupling pathways of the copper complex in turn feature significantly higher $\Delta H^{0\ddagger}$ values of 190, 168 and 196 kJ mol^{-1}, respectively. For $[RAgMe_3]^-$, the DLPNO-CCSD(T)//PBE-D3BJ reaction barriers follow the same trend (Figures 5, Table S1). While homo coupling has the lowest barrier with 138 kJ mol^{-1}, the $\Delta H^{0\ddagger}$ value increases from *regular* (165 kJ mol^{-1}) to *trans-cyclic* (170 kJ mol^{-1}) to *cis-cyclic* (178 kJ mol^{-1}) to *outer-sphere* cross coupling (202 kJ mol^{-1}). The zero-point vibrational energies and entropies at 298.15 K of the PBE-D3BJ C−C coupling TS structures relative to the equilibrium geometry ($\Delta ZPVE^{\ddagger}$ and $\Delta S^{298\ddagger}$, respectively) are also very similar for $[RCuMe_3]^-$ and $[RAgMe_3]^-$ (Figure S6, Table S1). In both cases, $\Delta ZPVE$s‡ are ≈ -5 kJ mol^{-1} and $-T\Delta S^{298\ddagger}$ values (for $T = 298.15$ K) are close to 0 kJ mol^{-1} except for the *outer-sphere* cross coupling. For the latter, both complexes feature a $\Delta ZPVE^{\ddagger}$ of ≈ -10 kJ mol^{-1} and a $-T\Delta S^{298\ddagger}$ value of about -20 kJ mol^{-1} and thus, a rather loose TS.

As bond dissociation reactions of molecular ions typically do not feature a kinetic barrier, *i.e.*, the reverse process is barrierless,[40] we assume that the threshold energies for the conceivable direct dissociations of $[RCuMe_3]^-$ and $[RAgMe_3]^-$ are equivalent to the corresponding reaction energies, ΔH^0. Therefore, from a kinetic perspective, the bond dissociation energies and the C−C coupling reaction barriers of the $[RMMe_3]^-$ ions are analogous quantities. For both complexes, our DLPNO-CCSD(T)//PBE-D3BJ calculations predict the homolytic cleavage of the metal−allyl bond to be energetically less demanding than the dissociation of the most weakly bound methyl group (177 vs. 214 kJ mol^{-1} for M = Cu; 169 vs. 183 kJ mol^{-1} for M = Ag; Figure 4, Table S2), which reflects the relative stability of the methyl and allyl radicals.[41] In a subsequent endothermic step, the $[MMe_3]^{\cdot-}$ species can lose a methyl radical, which requires an additional energy of 33 kJ mol^{-1} for M = Cu, but only 7 kJ mol^{-1} for M = Ag. The $[RMMe_2]^{\cdot-}$ complexes, in turn, can either also dissociate towards $[MMe_2]^-$ or lose another methyl radical. The latter process, again, is endothermic (30 kJ mol^{-1} for M = Cu; 26 kJ mol^{-1} for M = Ag), while the formation of $[MMe_2]^-$ appears to be energetically slightly downhill in both cases.[42] Consequently, according to the DLPNO-CCSD(T)//PBE-D3BJ calculations, the $[RMMe_2]^{\cdot-}$ species are not stable and hence, not accessible. Please note that the ΔH^0(PBE-D3BJ) values for the allyl radical loss of the $[RMMe_2]^{\cdot-}$ complexes are positive, and thus, obtaining energy minima for the $[RMMe_2]^{\cdot-}$ ions with the PBE-D3BJ method does not imply that the considered dissociation reactions feature a kinetic barrier. In essence, the energy diagrams for the twofold consecutive homolytic bond dissociations of $[RCuMe_3]^-$ and $[RAgMe_3]^-$ (Figure 4) indicate that the loss of an allyl radical is the only feasible homolytic dissociation pathway for these complexes and that the subsequent dissociation of the resulting $[MMe_3]^{\cdot-}$ ions towards $[MMe_2]^-$ features only a low activation energy. Furthermore, the calculated ΔH^0 values for the heterolytic dissociations of $[RMMe_3]^-$ are significantly higher than that for the loss of R$^{\cdot}$ (about 70 and 100 kJ mol^{-1} for M = Cu, Ag, respectively; Table S2).This

finding suggests that the formation of neutral fragment complexes upon collisional activation of isolated $[RMMe_3]^-$ species can be excluded.

Transferring the DLPNO-CCSD(T)//PBE-D3BJ reaction energies for the twofold homolytic bond dissociations of $[RMMe_3]^-$ to their C−C coupling reactivities shows that for both M = Cu and Ag, the bond-breaking part requires about 35 kJ mol^{-1} less energy for cross than for homo coupling (210 vs. 244 kJ mol^{-1} for M = Cu; 176 vs. 210 kJ mol^{-1} for M = Ag), which highlights the homologous character of the reactant and the product complexes. However, the energy release associated with the Me$^{\cdot}$/Me$^{\cdot}$ recombination is 60 kJ mol^{-1} higher than for the R$^{\cdot}$/Me$^{\cdot}$ recombination (Table S2) and thus, homo coupling is thermodynamically favored for both complexes (see Figure S7 for thermochemical cycles). Moreover, since the dissociation energy of the C−C bonds (367 and 307 kJ mol^{-1} for Me−Me and R−Me, respectively)[43,44] is much larger than the reaction energy for the twofold homolytic bond dissociations of $[RMMe_3]^-$, the C−C coupling reactions of the latter are highly exothermic, which is even more pronounced for M = Ag because of the energetically less demanding metal−carbon bond dissociations in this case.[45–47] A comparison between the calculated reaction barriers and the thermochemistry for the C−C coupling pathways of $[RCuMe_3]^-$ and $[RAgMe_3]^-$ reveals that homo coupling as the more exothermic reaction involves the lowest barrier for both complexes, which is also well below the threshold energy for the loss of R$^{\cdot}$ (Figure 5). Accordingly, the stability of the formed C−C bond seems to be the crucial factor for the difference between the reaction barriers for homo and cross coupling. In contrast to the correlation between thermochemistry and barrier heights for the homo- and cross-coupling reactions of $[RMMe_3]^-$, the DLPNO-CCSD(T)//PBE-D3BJ calculations predict higher reaction barriers for homo and *regular* cross coupling for M = Ag, although these C−C coupling reactions are more exothermic than for M = Cu. This trend indicates that the silver centre mediates the usual coupling mechanism less efficiently than copper, which has also been reported previously for neutral $[LMMe_3]$ and $[RMMe_2]$ complexes (M =Cu, Ag; L = PMe_3; R = allyl).[11,12] The latter, in combination with the slightly weaker M−R bond of $[RMMe_3]^-$ for M = Ag, causes a lower energy gap between the reaction barriers of the conventional C−C coupling pathways and the threshold energy for the allyl radical loss for the silver complex (Figure 5).

Rather peculiar is the result that the barrier for the *outer-sphere* cross coupling of $[RAgMe_3]^-$ is significantly higher (26 kJ mol^{-1}) than the threshold energy for the combined R$^{\cdot}$ and Me$^{\cdot}$ dissociation, which is not the case for the other cross-coupling pathways (also not for those of the $[RCuMe_3]^-$ complex). Given that the *outer-sphere* mechanism resembles a partial dissociation of the allyl ligand, which then abstracts a weakly bound methyl group in the course of the formation of a very stable C−C bond, one would expect that the energy of the corresponding TS structure lies below the dissociation limit of the twofold radical loss. Thus, the question arises whether the DLPNO-CCSD(T) method describes the electronic structure of the *outer-sphere* cross-coupling TS of $[RAgMe_3]^-$ correctly. Such a discrepancy could originate from a pronounced multi-configurational character of this transient species.

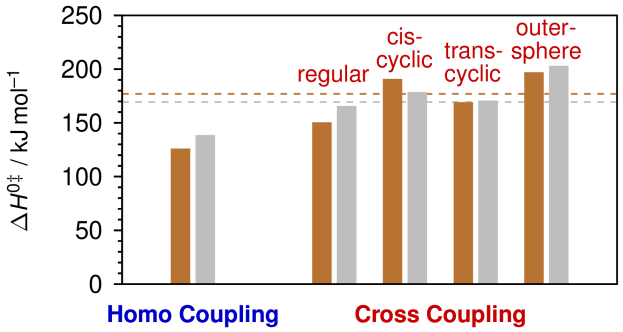

Figure 5. Reaction barriers for the homo- and cross-coupling pathways of $[RCuMe_3]^-$ and $[RAgMe_3]^-$ (copper- and silver-colored, respectively; R = η^1-allyl) obtained from DLPNO-CCSD(T)//PBE-D3BJ calculations. The dashed lines indicate the DLPNO-CCSD(T)//PBE-D3BJ threshold energies for the homolytic cleavage of the M−R bond of the complexes, which is the energetically most favorable dissociation reaction according to the coupled cluster calculations.

Multi-Configurational Calculations

In order to verify the applicability of the DLPNO-CCSD(T) method for the theoretical characterization of the unimolecular reaction space of the $[RMMe_3]^-$ complexes and in particular, to investigate whether the electronic structure of the *outer-sphere* TS for M = Ag indeed requires a multi-configurational (MC) treatment, we carried out MC perturbation theory calculations. The active orbital spaces of the underlying complete active space self-consistent field (CASSCF) calculations[48–51] were selected guided by a recently introduced automated protocol based on an orbital entanglement analysis.[52–55] Details on the selection process and all MC calculations are described in the Supporting Information. From the perspective of the equilibrium structure of $[RMMe_3]^-$, the final active space includes the four σ/σ^*-pairs of the metal-ligand bonds, an additional π/π^*-allyl orbital-pair, as well as as a double-shell $d_{x^2-y^2}$-orbital in case of M = Cu, where the lobes point towards the ligands, to arrive at active spaces with ten electrons in eleven and ten orbitals for M = Cu and Ag, respectively. The fact that double-shell orbitals are significantly entangled — and therefore relevant for the active space — only for the late 3d-metals and not for the homologous 4d-metals has been documented before.[53,56,57] Following the common CAS(N,L) notation with the number of active electrons N, and the number of active orbitals L, we denote these active spaces CAS(10,11) in case of copper, and CAS(10,10) in case of silver (pictures of the final set of orbitals are shown in Figures S8 and S9). This selection ensures a consistent active space for all $[RMMe_3]^-$ species and corresponding dissociation products discussed here and therefore guarantees size-consistency. For $[RCuMe_3]^-$, results from density matrix renormalization group[58–71] calculations with an even larger active space (CAS(18,20); Table S3) are discussed in the Supporting Information. To analyze the MC character of the converged CASSCF wave functions for the important species of this study, *viz.* the $[RMMe_3]^-$ equilibrium and TS structures as well as the $[MMe_3]^{\cdot-}$ fragment complexes, we determined their orbital entanglement based $Z_{s(1)}$ diagnostic[72] (Table 1; for corresponding mutual information diagrams, see Figures S10 and S11). $Z_{s(1)}$ can take values from 0 to 1, where $Z_{s(1)} = 0$ signals a pure single-configurational wave function (*i.e.* a Hartree–Fock wave function), whereas $Z_{s(1)} = 1$ is calculated for a hypothetical MC wave function where each orbital occupation of the active orbitals is equally realized. A value of $Z_{s(1)} > 0.2$ indicates a wave function that is likely to be poorly described by single-configurational approaches. The equilibrium and homo-coupling TS structures as well as the *regular* cross-coupling TS are single-configurational according to the $Z_{s(1)}$ diagnostic for both metals, whereas the higher values for the other TSs indicate a more pronounced MC character. Especially the *outer-sphere* TS structure of the silver complex has a remarkably large MC character, which is a strong indication that the corresponding barrier height is poorly calculated with a single-configurational method.

In Figure 6 Panel A, we show the reaction barriers for the homo-coupling and the different cross-coupling pathways for both $[RMMe_3]^-$ complexes, calculated with MC perturbation theory at second order, CASPT2,[73] without the so-called empirical IPEA shift as recommended by Zobel *et al.*[74] (values are given in Table S4, for more information on the IPEA shift, see the Supporting Information). Similar to Figure 5, the dashed horizontal lines indicate the threshold energies for the homolytic dissociation of the M−R bonds. In case of $[RAgMe_3]^-$, this energy is now almost equal to that of the *outer-sphere* TS structure in contrast to the DLPNO-CCSD(T) calculations, but in line with our expectations (*vide supra*). Panel B of Figure 6 shows the difference of the CASPT2 reactions barriers with respect to the coupled-cluster calculations. Interestingly, the CASPT2 energies are slightly larger for those TS structures with a small $Z_{s(1)}$ diagnostic whereas they are smaller for those with large MC character in case of the silver complex. The latter is especially

pronounced for the highly MC *outer-sphere* TS. This trend clearly indicates that the DLPNO-CCSD(T) approach overestimates the relative energies of the $[RAgMe_3]^-$ TS structures featuring a distinct MC character, where MC perturbation theory calculations are certainly more accurate than single-configurational coupled-cluster calculations. We therefore argue that while the single-configurational TS energies are accurate for those TS structures with negligible MC character, they become less trustworthy for the cross-coupling TSs with pronounced MC character, for which we deem the CASPT2 energies more reliable. This assessment is mainly relevant in case of Ag, where the much more pronounced quantitative discrepancies between the CASPT2 and DLPNO-CCSD(T) C−C coupling reaction barriers also go along with qualitatively different results for the two methods. More specifically, the CASPT2 calculations do not predict homo coupling as the energetically clearly most favorable reaction channel for the silver complex, whereas homo coupling features the by far lowest reaction barrier for $[RCuMe_3]^-$ independent of the electronic-structure method. However, the CASPT2 threshold energy for the allyl radical loss of the copper complex is significantly higher in comparison to the DLPNO-CCSD(T) result, which is not the case for the homolytic dissociation of the Ag−R bond. The reason for the discrepancy in case of copper is not obvious, but since the species involved in the $R^{\cdot}$ loss reaction have no pronounced MC character for both complexes, the corresponding coupled-cluster threshold energies are certainly more accurate. Moreover, as the $Z_{s(1)}$ diagnostic indicates that DLPNO-CCSD(T) calculations are valid for describing the electronic structure of the $[RMMe_3]^-$ and $[MMe_3]^{\cdot -}$ complexes, the same most likely applies to the other copper- and silver-containing equilibrium structures considered in this study, reinforcing the validity of all reaction energies discussed in the previous section.

Finally, we investigated whether the outcome of the CASPT2 calculations is affected by the choice of the IPEA shift. Indeed, when applying an IPEA shift of 0.25 E_h, a significant increase of the reaction barriers was obtained for the C−C coupling pathways featuring TS structures with pronounced MC character, which correlates with the increased TS $Z_{s(1)}$ values (Figure S12, Table S4). Nevertheless, the qualitative differences between the DLPNO-CCSD(T) and CASPT2(IPEA = 0 E_h) results for the $[RAgMe_3]^-$ complex as detailed above are present in case of an IPEA shift of 0.25 E_h as well, even though not as distinct. This finding strengthens our conclusion regarding the limited reliability of the DLPNO-CCSD(T) barrier heights corresponding to TS structures with pronounced MC character, but also emphasizes the uncertainty associated with the CASPT2 approach for these systems. In addition, the dissociation energies provide an internal benchmark for our calculations that represent a strictly single-configurational regime as measured by the $Z_{s(1)}$ diagnostic. The fact that the dissociation energies calculated with an IPEA shift of 0.0 E_h are much closer to the DLPNO-CCSD(T) energies than those calculated with the standard IPEA shift of 0.25 E_h (Figures 6 and S12) further suggests to neglect this empirical parameter.

Table 1. Multi-configurational $Z_{s(1)}$ diagnostic for the equilibrium and C−C coupling transition state (TS) structures of $[RMMe_3]^-$ as well as for the $[MMe_3]^{\cdot -}$ fragment complex (M = Cu, Ag; R = η^1-allyl). The diagnostic was evaluated from the CAS(10,11) active space for M = Cu and the CAS(10,10) active space in case of M = Ag.

	$Z_{s(1)}$	
	M = Cu	M = Ag
$[RMMe_3]^-$		
Equilibrium	0.13	0.12
TS Homo-Coupling	0.11	0.10
TSs Cross-Coupling		
regular	0.14	0.15
cis-cyclic	0.32	0.27
trans-cyclic	0.30	0.32
outer-sphere	0.34	0.41
$[MMe_3]^{\cdot -}$	0.08	0.08

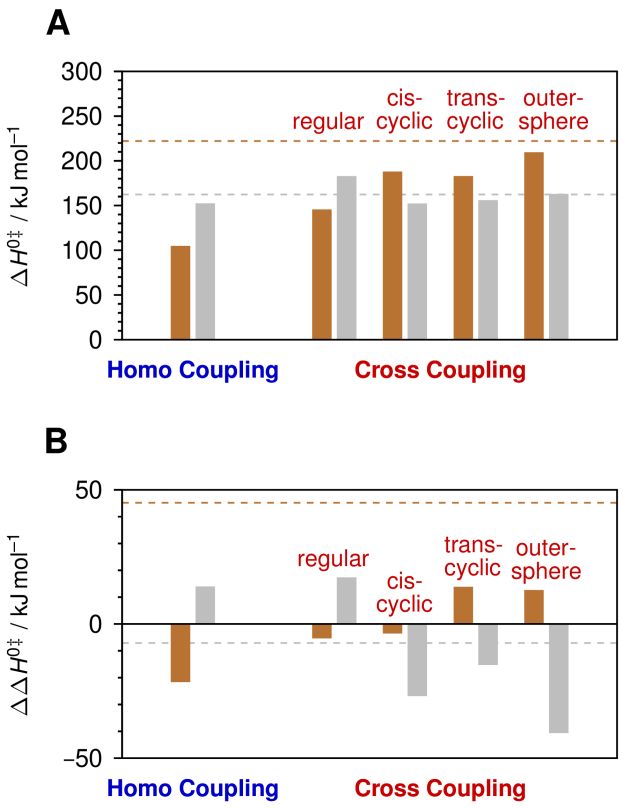

Figure 6. (A) Reaction barriers for the homo- and cross-coupling pathways of $[RCuMe_3]^-$ and $[RAgMe_3]^-$ (copper- and silver-colored, respectively; R = η^1-allyl) obtained from CASPT2(IPEA = 0 E_h)//PBE-D3BJ calculations. The dashed lines indicate the CASPT2(IPEA = 0 E_h)//PBE-D3BJ threshold energies for the homolytic cleavage of the M−R bond of the complexes, which is the energetically most favorable dissociation reaction according to DLPNO-CCSD(T)//PBE-D3BJ calculations. (B) The values from graph (A) are given relative to the corresponding DLPNO-CCSD(T)//PBE-D3BJ energies (cf. Figure 5).

Kinetic Calculations in Comparison with Experimental Results

The remaining key question is, whether the results of our quantum-chemical calculations are capable of correctly predicting the experimental outcome of the energy-dependent gas-phase fragmentation experiments on $[RCuMe_3]^-$ and $[RAgMe_3]^-$, and thus, of providing the explanation for the strikingly different reactivity of these two homologous transition-metal complexes. To this end, we determined microcanonical reaction rate constants, $k(E)$ by means of Rice–Ramsperger–Kassel–Marcus (RRKM) calculations for all theoretically identified C—C coupling pathways of both complexes as well as for their loss of an allyl radical as the only feasible direct dissociation according to the DLPNO-CCSD(T)//PBE-D3BJ results (for computational details, see the Supporting Information). The latter finding already implies that a collision-induced formation of $[RMMe]^-$ can only be attributed to the occurrence of homo coupling (Eq. 1a), whereas the observation of $[MMe_2]^-$ upon CID can either be the result of cross coupling (Eq. 2a) or of the transient formation of $[MMe_3]^{\cdot-}$ followed by a consecutive heterolytic M—Me bond dissociation (Eq. 2b). In this regard, it is also worth mentioning that studies on the unimolecular reactivity of $[RMMe]^-$ and $[MMe_2]^-$ from Rijs *et al.*[46,75] strongly argue against secondary fragmentations of these product complexes in the context of our CID experiments (for corresponding DLPNO-CCSD(T)//PBE-D3BJ bond dissociation energies, see Table S5). The therein calculated energy profiles are not only in agreement with the absence of $[RM]^{\cdot-}$, $[MMe]^{\cdot-}$ or $[HMMe]^-$ signals, but also emphasize that the obtained fragmentation spectra are not biased by R^- and Me^- loss reactions of the organometallate(I) complexes, which would not be detectable because of the m/z cutoff of the mass spectrometer used in this study.

For $[RCuMe_3]^-$, homo coupling features the highest $k(E)$ values within the experimentally relevant reaction rate constant range based on the RRKM calculations employing the DLPNO-CCSD(T)//PBE-D3BJ results for homo coupling, *regular* cross coupling and the $R^{\cdot}$ loss as well as the CASPT2(IPEA = 0 E_h)//PBE-D3BJ results for *cyclic* and *outer-sphere* cross coupling (Figure 7A; for details on the experimentally relevant reaction rate constant range, see the Supporting Information). Furthermore, none of the cross-coupling pathways is predicted to proceed fast enough to be observable within the conducted Q-TOF CID experiments. In contrast, considering the uncertainty with respect to the slope of the $k(E)$ curve for the $R^{\cdot}$ loss reaction as well as that of the experimental time scale τ, the RRKM calculations suggest that $[CuMe_3]^{\cdot-}$ is accessible upon collisional activation and that the homo-coupling/dissociation product ratio decreases with increasing collision energy. The latter results from the fact that the barrierless homolytic bond dissociation involves a loose, product-like and thus entropically favored TS, while the energetically less demanding homo coupling occurs *via* a much more rigid TS structure as indicated by the calculated $-T\Delta S^{298}$ and $-T\Delta S^{298\ddagger}$ values for the $R^{\cdot}$ loss and homo-coupling reactions, respectively (-58 vs. -3 kJ mol^{-1}; Figures 4 and S4). Also for entropic reasons, the slope of the $k(E)$ curve for the *outer-sphere* cross-coupling pathway ($-T\Delta S^{298\ddagger} = -22$ kJ mol^{-1}) is considerably steeper than for homo coupling. The theoretical predictions are directly consistent with two experimental observations, *viz.* the occurrence of $[RCuMe]^-$ as the main fragment ion at lower collisions energies as well as the detection of $[CuMe_3]^{\cdot-}$ (Figure 2A). Moreover, the RRKM calculations can also explain the decrease of the $[RCuMe]^-/[CuMe_2]^-$ product ratio with increasing collision energy. While they exclude a significant cross-coupling reactivity of $[RCuMe_3]^-$ within the performed gas-phase fragmentation experiments, they suggest that the $R^{\cdot}$ loss becomes more favorable at higher collision energies. Under these conditions, a large proportion of the formed $[CuMe_3]^{\cdot-}$ ions is expected to undergo collisions that induce the secondary fragmentation towards $[CuMe_2]^-$, since this reaction

only requires 33 kJ mol^{-1} (DLPNO-CCSD(T)//PBE-D3BJ value), *i.e.*, less than a fifth of the energy of the initial dissociation. Consequently, according to the theoretical results, the formation of $[CuMe_2]^-$ must arise from the twofold consecutive bond dissociation *via* $[CuMe_3]^{\cdot-}$, which in turn rationalizes the decrease of the signal intensity of the latter with increasing collision energy. Whether the observation of $[CuMe_2]^-$ in the context of the QIT CID experiments on $[RCuMe_3]^-$ by Putau *et al.*[16] has the same origin is unclear. As QIT CID is associated with a τ about two orders of magnitude larger than that of Q-TOF CID,[20,21] *regular* cross coupling could be faster than the allyl radical loss within the experimental relevant reaction rate constant range of the former based on the calculated $k(E)$ curves. Support for this scenario it the lack of $[CuMe_3]^{\cdot-}$ fragment ions in the previous study, but it is also possible that this labile species is indeed formed and just does not survive the way to the detector, given that it will undergo many collisions and has considerable reaction time available in the QIT mass spectrometer. The deviating progression of the $[RCuMe]^-/[CuMe_2]^-$ product ratios with increasing energy for the two experimental setups, however, should not necessarily be interpreted as indication for the occurrence of different $[CuMe_2]^-$ formation reactions, because the product ratio difference can merely be the result of the different energy ranges probed by the two instruments.

If the CASPT2(IPEA = 0.25 E_h)//PBE-D3BJ or DLPNO-CCSD(T)//PBE-D3BJ results are used in the RRKM calculations for *cyclic* and *outer-sphere* cross coupling of $[RCuMe_3]^-$ instead of those obtained from the CASPT2(IPEA = 0 E_h)//PBE-D3BJ approach, the corresponding $k(E)$ curves are shifted to even higher or slightly lower energies, respectively, which does not affect the theoretical predictions for the unimolecular reactivity of this species (Figures S13 and S14). Thus, there is no indication that these pathways play a role with respect to the $[CuMe_2]^-$ formation upon collisional activation of the copper complex. Additionally, the $k(E)$ values for $[RCuMe_3]^-$ calculated only on the basis of the CASPT2//PBE-D3BJ results are not in accordance with the experimental observations, because they imply homo coupling as the only possible reaction (Figure S15). This finding emphasizes that the CASPT2 method is at least not appropriate for an accurate description of the potential energy surface underlying the reaction channels of the cuprate(III) species that do not involve structures with pronounced multi-configurational character.

RRKM theory employing the results from DLPNO-CCSD(T)//PBE-D3BJ calculations for homo coupling, *regular* cross coupling and the R$^{\cdot}$ loss as well as from CASPT2(IPEA = 0 E_h)//PBE-D3BJ calculations for *cyclic* and *outer-sphere* cross coupling predicts a distinctly different CID reactivity for $[RAgMe_3]^-$ compared to its copper analogue. Taking into account the theoretical uncertainty with respect to the allyl radical loss in combination with the experimental uncertainty in τ, the calculated $k(E)$ values for the silver complex suggest that the direct dissociation could be faster than any C−C coupling reaction within the the experimentally relevant reaction rate range and thus constitute the dominant channel (Figure 7A). At the same time, the kinetic calculations indicate that a competition between homo coupling and the R$^{\cdot}$ loss reaction can be expected to take place and that the dissociation/homo-coupling product ratio increases with increasing collision energy in line with the entropic characteristics of these processes (Figures 4 and S5). Furthermore, the occurrence of the entropically favorable *outer-sphere* cross coupling reaction might be possible as well based on the RRKM results, although only to a limited extent, whereas this is not the case for the other cross-coupling pathways. As with $[RCuMe_3]^-$, the theoretical predictions for the unimolecular reactivity of the silver complex are also in accordance with the experimental findings. On the one hand, $[RAgMe]^-$ and hence, homo coupling indeed was observed upon collisional activation (Figure 2B). On the other hand, considering that only 7 kJ mol^{-1} (DLPNO-

CCSD(T)//PBE-D3BJ value) are required for the secondary fragmentation of $[AgMe_3]^{\cdot -}$ towards $[AgMe_2]^-$, it is plausible that the former, because of its lability, was not detected within our Q-TOF CID experiments. This would mean that every $R^{\cdot}$ loss reaction is accompanied by the formation of $[AgMe_2]^-$, which rationalizes that the latter is the main product upon collisional activation and that the $[AgMe_2]^-/[RAgMe]^-$ product increases with increasing collision energy. If the observed $[AgMe_2]^-$ ion at least partially originates from *outer-sphere* cross coupling, however, can neither be confirmed nor excluded by means of the kinetic calculations outlined above.

Upon application of the CASPT2(IPEA = 0.25 E_h)//PBE-D3BJ or DLPNO-CCSD(T)//PBE-D3BJ results for *cyclic* and *outer-sphere* cross coupling of $[RAgMe_3]^-$ (rather than those from the CASPT2(IPEA =0 E_h)//PBE-D3BJ calculations), $k(E)$ curves were obtained that do not ascribe the experimental detection of $[AgMe_2]^-$ to any cross-coupling reactivity (Figures S13 and S14). In contrast, the RRKM calculations on the basis of the CASPT2//PBE-D3BJ results for all considered pathways do not rule out that *outer-sphere* cross coupling might contribute to the formation of $[AgMe_2]^-$ (Figure S15). However, dependent on the employed IPEA shift, the CASPT2//PBE-D3BJ results are associated with $k(E)$ values that under- (IPEA =0 E_h) or rather overestimate (IPEA =0.25 E_h) the occurrence of homo coupling in comparison with the CID experiments. Accordingly, also for the silver complex, the CASPT2 approach provides a less trustworthy gap between the homo coupling reaction barrier and the $R^{\cdot}$ loss threshold energy than DLPNO-CCSD(T), although the discrepancy between the two methods is less here compared to that for $[RCuMe_3]^-$. Altogether, the kinetic calculations for the argentate(III) complex consistently suggest that the predominant fragmentation of this species towards $[AgMe_2]^-$ upon collisional activation arises from a twofold consecutive homolytic bond dissociation. Therefore, they highlight that considering this type of reaction can be crucial for the correct interpretation of CID experiments that point to C−C coupling reactivity because of the absence of the transient direct dissociation product.

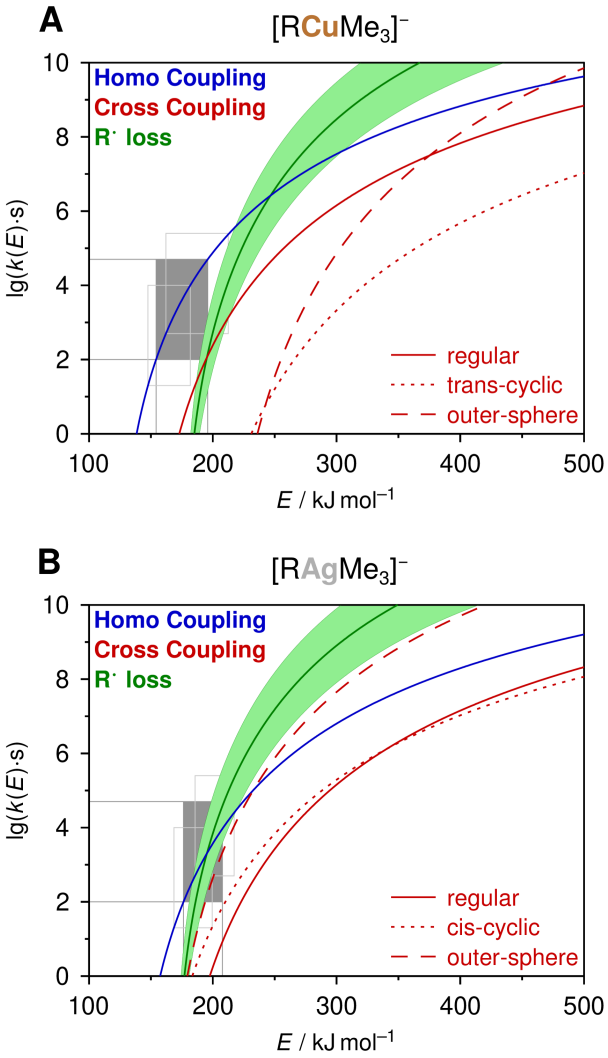

Figure 7. Microcanonical reaction rate constants for the homo- and cross-coupling pathways of (A) $[RCuMe_3]^-$ and (B) $[RAgMe_3]^-$ (R = η^1-allyl) as well as for their loss of R$^\cdot$ obtained from RRKM theory employing results from DLPNO-CCSD(T)//PBE-D3BJ (homo and *regular* cross coupling, R$^\cdot$ loss) and CASPT2(IPEA = 0 E_h)//PBE-D3BJ calculations (*cyclic* and *outer-sphere* cross coupling). Estimated upper and lower limits of the $k(E)$ values for the R$^\cdot$ loss reactions define the green areas. The reaction rate constants within the filled gray boxes have to be considered for the theoretical prediction of the performed gas-phase fragmentation experiments under the assumption of an experimental time scale of $\tau = 10^{-4}$ s. To account for the uncertainty associated with τ, the lower and upper empty gray boxes indicate the relevant reaction rate constant ranges for $\tau = 5 \cdot 10^{-4}$ s and $2 \cdot 10^{-5}$ s, respectively. In each case, the $k(E)$ values for the *cyclic* cross-coupling pathway featuring the higher reaction barrier are not shown.

Origin of the Different Reactivity of $[RCuMe_3]^-$ and $[RAgMe_3]^-$

Since our theoretical predictions for the unimolecular reactivity of the gaseous $[RCuMe_3]^-$ and $[RAgMe_3]^-$ complexes are in compliance with the results of the gas-phase fragmentation experiments on these ions, the origin of their strikingly different behaviour upon collisional activation can finally be clarified. For the copper complex, homo coupling features a reaction barrier, which is considerably lower than that of the most favorable cross-coupling pathway, *i.e.*, *regular* cross coupling, and also than the threshold energy of the allyl radical loss reaction as the only feasible direct dissociation. Thus, this species mainly reacts towards $[RCuMe]^-$ at lower collision energies, while the formation of $[CuMe_2]^-$ relative to that of $[RCuMe]^-$ increases with increasing energy because the consecutive $R^{\cdot}/Me^{\cdot}$ loss becomes more favorable for entropic reasons. In the case of the silver complex, both the homo coupling and the *regular* cross coupling reaction barriers are consistently higher in comparison to the copper congener, but at the same time, the bond dissociation energy of the metal−allyl bond is slightly lower. In addition, the threshold energy for the $Me^{\cdot}$ loss of the $[AgMe_3]^{\cdot-}$ fragment ion is significantly lower than for $[CuMe_3]^{\cdot-}$. These bond dissociation energy considerations are in accordance with the result that the entropically favored *outer-sphere* cross-coupling pathway is associated with a much lower reaction barrier for $[RAgMe_3]^-$ compared to the copper analogue, which is similar to that for *regular* cross coupling of the former. As a consequence, the consecutive $R^{\cdot}/Me^{\cdot}$ loss of the argentate(III) complex is more favorable than homo coupling and hence $[AgMe_2]^-$ is observed as the major fragment ion within the corresponding CID experiments. However, it cannot be ruled out that at least a fraction of the detected $[AgMe_2]^-$ ions can be attributed to an *outer-sphere* cross-coupling reaction, which is mechanistically closely related to the twofold homolytic bond fission, since it involves the partial dissociation of the allyl ligand, which then aids the cleavage of a weak Ag−Me bond in the course of the C−C bond formation. In essence, for both $[RMMe_3]^-$ complexes, the kinetically preferred conventional reductive elimination pathway corresponds to the thermodynamically more favorable coupling reaction, *i.e.*, homo coupling, whereas the dissociative channels of these species go along with breaking of the metal−allyl bond, which either results in a consecutive $R^{\cdot}/Me^{\cdot}$ loss or an *outer-sphere* cross coupling. On this basis, the contrasting reactivity of the two coinage metallates can be traced back to the fact that the transition from copper to silver leads to a facilitation of the reactions featuring a dissociative character, because the Ag−organyl bonds are weaker and the silver centre mediates the regular C−C bond formation mechanism less efficiently.

The insights gained for the unimolecular reactivity of $[RAgMe_3]^-$ in the gas phase eventually allow for an interpretation of the 1-butene formation *via* this organoargentate species in THF as observed by NMR experiments.[7] It appears highly unlikely that the silver complex sequentially dissociates towards solvent-separated $[AgMe_2]^-$, $R^{\cdot}$, $Me^{\cdot}$ fragments, which is followed by a recombination of the two free radicals yielding 1-butene. Instead, the loss of an allyl radical may occur, which then recombines with the remaining $[AgMe_3]^{\cdot-}$ complex in such a way that 1-butene is formed or only a partial dissociation of the allyl ligand takes place, which then immediately abstracts a methyl group according to the *outer-sphere* cross coupling mechanism. As the presence of a solvent cage should favor the latter option and our theoretical results revealed that, even in the gas phase, this pathway could compete with the direct dissociation reaction, we propose that $[RAgMe_3]^-$ undergoes *outer-sphere* cross coupling in THF. Interestingly, for the allylic methylation reaction between $LiCuMe_2{\cdot}LiI$ and cinnamyl chloride, $[R^{Ph}CuMe_2]$ and $[R^{Ph}CuMe_3]^-$ (R^{Ph} = cinnamyl) were both characterized as reactive cross-coupling intermediates yielding 1-phenylbutene (S_N2 product) and 3-phenylbutene (S_N2' product), respectively.[13,15] The observed reactivity for the organocuprate(III)

complex has not been explained previously, but is consistent with the regioselectivity accompanied with the *outer-sphere* mechanism identified in this study. Hence, as reactions between organoargentate(I) compounds and substituted allylic halides are expected to proceed *via* ate(III) species,[7] they may yield cross-coupling products complementary to those accessible *via* their Cu-mediated analogues, which typically involve neutral organocopper(III) intermediates.[1,13]

Conclusions

Our energy-dependent gas-phase fragmentation experiments have unambiguously demonstrated that the homologous coinage metallate complexes $[RCuMe_3]^-$ and $[RAgMe_3]^-$ (R = η^1-allyl) exhibit a distinctly different behaviour upon collisional activation. While the former mainly produces $[RCuMe]^-$, the latter nearly exclusively reacts towards $[AgMe_2]^-$, which is in line with the previously observed cross-coupling reactivity of the argentate(III) species in solution. With the help of an extensive theoretical characterization of the unimolecular reactivity of the $[RMMe_3]^-$ ions, including DFT, DLPNO-CCSD(T) and CASPT2 calculations as well as the computation of RRKM reaction rate constants, a fundamental understanding of their chemistry was achieved. On the basis of DLPNO-CCSD(T)//PBE-D3BJ calculations, conceivable reaction pathways for both complexes are homo coupling, four different cross-coupling possibilities (*regular*, *cis-cyclic*, *trans-cyclic*, *outer-sphere*) and the loss of an allyl radical. We have shown that for the description of the electronic structure of the *cis-cyclic*, *trans-cyclic* and *outer-sphere* cross-coupling TSs, multireference calculations are required, which, in contrast to the DLPNO-CCSD(T) results, indicate that the reaction barriers of the corresponding channels are significantly lower for the silver than for the copper complex. Additionally, according to the DLPNO-CCSD(T) calculations, (i) $[RAgMe_3]^-$ mediates homo coupling less efficiently compared to its Cu analogue, where this reaction clearly features the lowest reaction barrier and (ii) the direct dissociations for the $[RMMe_3]^-$ species and the $[MMe_3]^{\cdot-}$ fragment ions are more favorable for M = Ag. Our kinetic computations employing the results from the quantum-chemical calculations are in good agreement with the observations from the gas-phase fragmentation experiments, which highlights the validity of the determined potential energy surfaces. The obtained reaction rate constants not only correctly predict the preference of the cuprate(III) complex to undergo homo coupling, which is the only feasible origin for the $[RCuMe]^-$ product ion, but can also rationalize that the silver congener predominantly produces $[AgMe_2]^-$, which most likely arises from a twofold consecutive homolytic bond dissociation. However, the *outer-sphere* cross-coupling reaction, which involves the partial dissociation of the allyl ligand before C—C coupling occurs, might also contribute to the $[AgMe_2]^-$ formation in the gas phase. As the *outer-sphere* mechanism corresponds to the most favorable cross-coupling pathway for $[RAgMe_3]^-$, we assume that this process underlays the solution-phase reactivity of the silver species. Altogether, the presented study unravels the intriguing differences between the reactivity of heteroleptic tetraalkylcuprate(III) and -argentate(III) complexes featuring allyl ligands in great detail and provides an improved mechanistic understanding of coinage metallate(III) mediated C—C coupling reactions, which in particular highlights the so far underestimated potential of silver for such transformations.

Supporting Information

Experimental details, computational details, mass spectra, further results from electronic structure calculations and further results from kinetic calculations (PDF)

XYZ coordinates (in Å) of all calculated structures and harmonic vibrational frequencies (in cm^{-1}) of the structures considered within the kinetic computations (ZIP).

Acknowledgments

T.A. and K.K. gratefully acknowledge support from the Deutsche Forschungsgemeinschaft, 389479699/GRK2455 and KO2875/12-1. C.J.S. acknowledges funding by the Ministry of Innovation, Science and Research of North Rhine-Westphalia ("NRW Rückkehrerprogramm"). C.J.S. thanks Prof. Markus Reiher (ETH Zürich) for computing time. R.A.J.O. thanks the Humboldt foundation for the award of a senior fellowship.

TOC Graphic

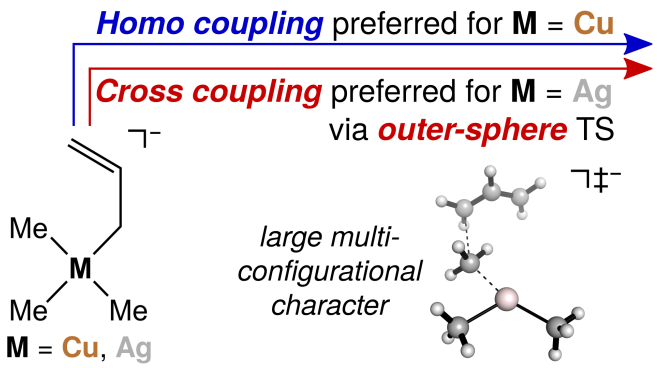

References

[1] Yoshikai, N.; Nakamura, E. Mechanisms of nucleophilic organocopper(i) reactions. *Chem. Rev.* **2012**, *112*, 2339-2372.

[2] Rappoport, Z., Marek, I., Eds. *The Chemistry of Organocopper Compounds;* Wiley: Hoboken, NJ, 2009.

[3] Weibel, J.-M.; Blanc, A.; Pale, P. Ag-mediated reactions: Coupling and heterocyclization reactions. *Chem. Rev.* **2008**, *108*, 3149-3173.

[4] Harmata, M., Ed. *Silver in Organic Chemistry;* Wiley: Hoboken, NJ, 2010.

[5] Font, M.; Acuña-Parés, F.; Parella, T.; Serra, J.; Luis, J. M.; Lloret-Fillol, J.; Costas, M.; Ribas, X. Direct observation of two-electron ag(i)/ag(iii) redox cycles in coupling catalysis. *Nat. Commun.* **2014**, *5*, 4373.

[6] Capdevila, L.; Andris, E.; Briš, A.; Tarrés, M.; Roldán-Gómez, S.; Roithová, J.; Ribas, X. Silver(i)-catalyzed c–x, c–c, c–n, and c–o cross-couplings using aminoquinoline directing group via elusive aryl-ag(iii) species. *ACS Catal.* **2018**, *8*, 10430-10436.

[7] Weske, S.; Hardin, R. A.; Auth, T.; O'Hair, R. A. J.; Koszinowski, K.; Ogle, C. A. Argentate(i) and (iii) complexes as intermediates in silver-mediated cross-coupling reactions. *Chem. Commun.* **2018**, *54*, 5086-5089.

[8] Tezuka, N.; Hirano, K.; Peel, A. J.; Wheatley, A. E. H.; Miyamoto, K.; Uchiyama, M. Lipshutz-type bis(amido)argentates for directed *ortho* argentation. *Chem. Sci.* **2020**, *11*, 1855-1861.

[9] Deuker, M.; Yang, Y. A.; O'Hair, R. A. J.; Koszinowski, K. Tetraorganylargentate(iii) complexes: Key intermediates in silver-mediated cross-coupling reactions. *Organometallics* **2021**, *40*, 2354-2363.

[10] Lu, Z.; Liu, S.; Lan, Y.; Leng, X.; Shen, Q. C(sp^2)-cf_3 reductive elimination from well-defined argentate(iii) complexes [nbu_4n][$ag(ar)(cf_3)_3$]. *Organometallics* **2021**, *40*, 1713-1718.

[11] Nakanishi, W.; Yamanaka, M.; Nakamura, E. Reactivity and stability of organocopper(i), silver(i), and gold(i) ate compounds and their trivalent derivatives. *J. Am. Chem. Soc.* **2005**, *127*, 1446-1453.

[12] Rijs, N. J.; Yoshikai, N.; Nakamura, E.; O'Hair, R. A. J. Gas-phase reactivity of group 11 dimethylmetallates with allyl iodide. *J. Am. Chem. Soc.* **2012**, *134*, 2569-2580.

[13] Bartholomew, E. R.; Bertz, S. H.; Cope, S.; Murphy, M.; Ogle, C. A. Preparation of σ- and π-allylcopper(iii) intermediates in s_N2 and s_N2' reactions of organocuprate(i) reagents with allylic substrates. *J. Am. Chem. Soc.* **2008**, *130*, 11244-11245.

[14] Hickman, A. J.; Sanford, M. S. High-valent organometallic copper and palladium in catalysis. *Nature* **2012**, *484*, 177-185.

[15] Casitas, A.; Ribas, X. The role of organometallic copper(iii) complexes in homogeneous catalysis. *Chem. Sci.* **2013**, *4*, 2301-2318.

[16] Putau, A.; Brand, H.; Koszinowski, K. Tetraalkylcuprates(iii): Formation, association, and intrinsic reactivity. *J. Am. Chem. Soc.* **2012**, *134*, 613-622.

[17] The reason why the [$RMMe_2$] species is only formed in THF solutions of $LiMMe_2$·LiI and RX for M = Cu, and not for M = Ag (X = Cl, I for M = Cu, Ag, respectively) is unclear.

[18] Yamanaka, M.; Kato, S.; Nakamura, E. Mechanism and regioselectivity of reductive elimination of π-allylcopper (iii) intermediates. *J. Am. Chem. Soc.* **2004**, *126*, 6287-6293.

[19] Yoshikai, N.; Zhang, S.-L.; Nakamura, E. Origin of the regio- and stereoselectivity of allylic substitution of organocopper reagents. *J. Am. Chem. Soc.* **2008**, *130*, 12862-12863.

[20] McLuckey, S. A.; Goeringer, D. E. Slow heating methods in tandem mass spectrometry. *J Mass Spectrom.* **1997**, *32*, 461-474.

[21] Wells, J. M.; McLuckey, S. A. Collision-Induced Dissociation (CID) of Peptides and Proteins. In *Methods in Enzymology*; Biological Mass Spectrometry; Academic Press: 2005; 402, pp 148-185.

[22] For investigations on reductive elimination reactions of related copper(III) complexes, see Paeth *et al.*[23] and Liu *et al.*[24].

[23] Paeth, M.; Tyndall, S. B.; Chen, L.-Y.; Hong, J.-C.; Carson, W. P.; Liu, X.; Sun, X.; Liu, J.; Yang, K.; Hale, E. M.; Tierney, D. L.; Liu, B.; Cao, Z.; Cheng, M.-J.; Goddard III, W. A.; Liu, W. Csp^3—csp^3 bond-forming reductive elimination from well-defined copper(iii) complexes. *J. Am. Chem. Soc.* **2019**, *141*, 3153-3159.

[24] Liu, S.; Liu, H.; Liu, S.; Lu, Z.; Lu, C.; Leng, X.; Lan, Y.; .; Shen, Q. C(sp^3)-cf_3 reductive elimination from a five-coordinate neutral copper(iii) complex. *J. Am. Chem. Soc.* **2020**, *142*, 9785-9791.

[25] For investigations on twofold consecutive homolytic bond dissociations of related copper(III) and silver(III) complexes, see Baya *et al.*[26].

[26] Baya, M.; Joven-Sancho, D.; Alonso, P. J.; Orduna, J.; Menjón, B. M—c bond homolysis in coinage-metal $[m(cf_3)_4]^-$ derivatives. *Angew. Chem. Int. Ed.* **2019**, *58*, 9954-9958.

[27] Baya, M.; Joven-Sancho, D.; Alonso, P. J.; Orduna, J.; Menjón, B. M—c bond homolysis in coinage-metal $[m(cf_3)_4]^-$ derivatives. *Angew. Chem. Int. Ed.* **2020**, *59*, 2544.

[28] Perdew, J. P.; Burke, K.; Ernzerhof, M. Generalized gradient approximation made simple. *Phys. Rev. Lett.* **1996**, *77*, 3865-3868.

[29] Perdew, J. P.; Burke, K.; Ernzerhof, M. Generalized gradient approximation made simple [phys. rev. lett. 77, 3865 (1996)]. *Phys. Rev. Lett.* **1997**, *78*, 1396-1396.

[30] Grimme, S.; Antony, J.; Ehrlich, S.; Krieg, H. A consistent and accurate ab initio parametrization of density functional dispersion correction (dft-d) for the 94 elements h-pu. *J. Chem. Phys.* **2010**, *132*, 154104.

[31] Grimme, S.; Ehrlich, S.; Goerigk, L. Effect of the damping function in dispersion corrected density functional theory. *J. Comput. Chem.* **2011**, *32*, 1456-1465.

[32] Other *outer-sphere* mechanisms relevant to metal-mediated C—X coupling reactions have been reported and include radical processes (see Sharma *et al.*[33]) or a stepwise reductive elimination consisting of the dissociation of an anion, which then attacks another ligand bound to the metal in a S_N2 fashion (see Yu *et al.*[34]).

[33] Sharma, A. K.; Sameera, W. M. C.; Jin, M.; Adak, L.; Okuzono, C.; Iwamoto, T.; Kato, M.; Nakamura, M.; Morokuma, K. Dft and afir study on the mechanism and the origin of enantioselectivity in iron-catalyzed cross-coupling reactions. *J. Am. Chem. Soc.* **2017**, *139*, 16117-16125.

[34] Yu, J.-L.; Zhang, S.-Q.; Hong, X. Stepwise versus concerted reductive elimination mechanisms in the carbon—iodide bond formation of (dpephos)rhmei$_2$ complex. *Organometallics* **2018**, *37*, 4711-4719.

[35] Snyder, J. P. Mechanism of lithium cuprate conjugate addition: Neutral tetracoordinate cui cuprates as essential intermediates. *J. Am. Chem. Soc.* **1995**, *117*, 11025-11026.

[36] Dorigo, A. E.; Wanner, J.; von Ragué Schleyer, P. Computational evidence for the existence of cu^{III} intermediates in addition and substitution reactions with dialkylcuprates. *Angew. Chem. Int. Ed. Engl.* **1995**, *34*, 476-478.

[37] Riplinger, C.; Neese, F. An efficient and near linear scaling pair natural orbital based local coupled cluster method. *J. Chem. Phys.* **2013**, *138*, 034106.

[38] Riplinger, C.; Sandhoefer, B.; Hansen, A.; Neese, F. Natural triple excitations in local coupled cluster calculations with pair natural orbitals. *J. Chem. Phys.* **2013**, *139*, 134101.

[39] Riplinger, C.; Pinski, P.; Becker, U.; Valeev, E. F.; Neese, F. Sparse maps—a systematic infrastructure for reduced-scaling electronic structure methods. ii. linear scaling domain based pair natural orbital coupled cluster theory. *J. Chem. Phys.* **2016**, *144*, 024109.

[40] Armentrout, P. B.; Ervin, K. M.; Rodgers, M. T. Statistical rate theory and kinetic energy-resolved ion chemistry: Theory and applications. *J. Phys. Chem. A* **2008**, *112*, 10071-10085.

[41] Henry, D. J.; Parkinson, C. J.; Mayer, P. M.; Radom, L. Bond dissociation energies and radical stabilization energies associated with substituted methyl radicals. *J. Phys. Chem. A* **2001**, *105*, 6750-6756.

[42] According to our DLPNO-CCSD(T)//PBE-D3BJ calculations, $[MMe_3]^{\cdot-}$ and $[RMMe_2]^{\cdot-}$ complexes (M = Cu, Ag; R = η^1-allyl) are stable with respect to electron loss – for the former, the corresponding ΔH^0 values are 111 and 136 kJ mol^{-1} for M =Cu and Ag, respectively; for the latter, the corresponding ΔH^0 values are 36 and 91 kJ mol^{-1} for M =Cu and Ag, respectively.

[43] The calculated C−C bond dissociation energies for Me−Me and R−Me (R = allyl) are in good agreement with the experimentally determined values reported by Blanksby and Ellison[44].

[44] Blanksby, S. J.; Ellison, G. B. Bond dissociation energies of organic molecules. *Acc. Chem. Res.* **2003**, *36*, 255-263.

[45] Calculations of Rijs *et al.*[46,47] have shown that also for [MR] and [RMMe]$^-$ complexes (M =Cu, Ag), the M−organyl bonds are consistently weaker in the case of M = Ag.

[46] Rijs, N. J.; O'Hair, R. A. J. Unimolecular reactions of organocuprates and organoargentates. *Organometallics* **2010**, *29*, 2282-2291.

[47] Rijs, N. J.; Brookes, N. J.; O'Hair, R. A. J.; Yates, B. F. Theoretical approaches to estimating homolytic bond dissociation energies of organocopper and organosilver compounds. *J. Phys. Chem. A* **2012**, *116*, 8910-8917.

[48] Roos, B. O.; Taylor, P. R.; Siegbahn, P. E. A complete active space scf method (casscf) using a density matrix formulated super-ci approach. *Chem. Phys.* **1980**, *48*, 157-173.

[49] Werner, H.-J.; Knowles, P. J. A second order multiconfiguration scf procedure with optimum convergence. *J. Chem. Phys.* **1985**, *82*, 5053-5063.

[50] Roos, B. O. The complete active space self-consistent field method and its applications in electronic structure calculations. *Adv. Chem. Phys.* **1987**, *69*, 399-445.

[51] Shepard, R. The multiconfiguration self-consistent field method. *Adv. Chem. Phys.* **1987**, *69*, 63-200.

[52] Stein, C. J.; Reiher, M. Automated Selection of Active Orbital Spaces. *J. Chem. Theory Comput.* **2016**, *12*, 1760-1771.

[53] Stein, C. J.; von Burg, V.; Reiher, M. The delicate balance of static and dynamic electron correlation. *J. Chem. Theory Comput.* **2016**, *12*, 3764-3773.

[54] Stein, C. J.; Reiher, M. Automated identification of relevant frontier orbitals for chemical compounds and processes. *Chimia* **2017**, *71*, 170-176.

[55] Stein, C. J.; Reiher, M. autocas: A program for fully automated multiconfigurational calculations. *J. Comput. Chem.* **2019**, *40*, 2216-2226.

[56] Pierloot, K. Nondynamic Correlation Effects in Transition Metal Coordination Compounds. In *Computational Organometallic Chemistry*; Cundari, T. R., Ed.; Marcel Dekker, Inc.: 2001; pp 123-158.

[57] Freitag, L.; Knecht, S.; Keller, S. F.; Delcey, M. G.; Aquilante, F.; Bondo Pedersen, T.; Lindh, R.; Reiher, M.; Gonzalez, L. Orbital entanglement and casscf analysis of the ru–no bond in a ruthenium nitrosyl complex. *Phys. Chem. Chem. Phys.* **2015**, *17*, 14383-14392.

[58] White, S. R. Density matrix formulation for quantum renormalization groups. *Phys. Rev. Lett.* **1992**, *69*, 2863-2866.

[59] White, S. R. Density-matrix algorithms for quantum renormalization groups. *Phys. Rev. B* **1993**, *48*, 10345-10356.

[60] Legeza, Ö.; Noack, R.; Sólyom, J.; Tincani, L. Applications of quantum information in the density-matrix renormalization group. *Lect. Notes Phys.* **2008**, *739*, 653-664.

[61] Chan, G. K.-L.; Dorando, J. J.; Ghosh, D.; Hachmann, J.; Neuscamman, E.; Wang, H.; Yanai, T. An introduction to the density matrix renormalization group ansatz in quantum chemistry. *Prog. Theor. Chem. Phys.* **2008**, *18*, 49-65.

[62] Chan, G. K.-L.; Zgid, D. The density matrix renormalization group in quantum chemistry. **2009**, *5*, 149-162.

[63] Marti, K. H.; Reiher, M. The density matrix renormalization group algorithm in quantum chemistry. *Z. Phys. Chem.* **2010**, *224*, 583-599.

[64] Schollwöck, U. The density-matrix renormalization group in the age of matrix product states. *Annals of Physics* **2011**, *326*, 96-192.

[65] Chan, G. K.-L.; Sharma, S. The density matrix renormalization group in chemistry. *Ann. Rev. Phys. Chem.* **2011**, *62*, 465.

[66] Marti, K. H.; Reiher, M. New electron correlation theories for transition metal chemistry. *Phys. Chem. Chem. Phys.* **2011**, *13*, 6750-6759.

[67] Wouters, S.; Van Neck, D. The density matrix renormalization group for ab initio quantum chemistry. *Eur. Phys. J. D* **2014**, *68*, 272.

[68] Yanai, T.; Kurashige, Y.; Mizukami, W.; Chalupský, J.; Lan, T. N.; Saitow, M. Density matrix renormalization group for ab initio calculations and associated dynamic correlation methods: A review of theory and applications. *Int. J. Quantum Chem.* **2015**, *115*, 283-299.

[69] Szalay, S.; Pfeffer, M.; Murg, V.; Barcza, G.; Verstraete, F.; Schneider, R.; Legeza, Ö. Tensor product methods and entanglement optimization for ab initio quantum chemistry. *Int. J. Quantum Chem.* **2015**, *115*, 1342-1391.

[70] Chan, G. K.-L.; Keselman, A.; Nakatani, N.; Li, Z.; White, S. R. Matrix product operators, matrix product states, and ab initio density matrix renormalization group algorithms. *J. Chem. Phys.* **2016**, *145*, 014102.

[71] Knecht, S.; Hedegård, E. D.; Keller, S.; Kovyrshin, A.; Ma, Y.; Muolo, A.; Stein, C. J.; Reiher, M. New approaches for ab initio calculations of molecules with strong electron correlation. *Chimia* **2016**, *70*, 244-251.

[72] Stein, C. J.; Reiher, M. Measuring multi-configurational character by orbital entanglement. *Mol. Phys.* **2017**, *115*, 2110-2119.

[73] Andersson, K.; Malmqvist, P. Å.; Roos, B. O. Second-order perturbation theory with a complete active space self-consistent field reference function. *J. Chem. Phys.* **1992**, *96*, 1218-1226.

[74] Zobel, J. P.; Nogueira, J. J.; González, L. The ipea dilemma in caspt2. *Chem. Sci.* **2017**, *8*, 1482-1499.

[75] Rijs, N. J.; Yates, B. F.; O'Hair, R. A. J. Dimethylcuprate undergoes a dyotropic rearrangement. *Chem. Eur. J.* **2010**, *16*, 2674-2678.